photonics

MDPI

Article

Perovskite Nanocrystal-Coated Inorganic Scintillator-Based Fiber-Optic Gamma-ray Sensor with Higher Light Yields

Seokhyeon Jegal [1], Siwon Song [1], Jae Hyung Park [1], Jinhong Kim [1], Seunghyeon Kim [1], Sangjun Lee [1], Cheol Ho Pyeon [2], Sin Kim [1] and Bongsoo Lee [1,*]

[1] School of Energy System Engineering, Chung-Ang University, Seoul 06974, Republic of Korea; scr1501@cau.ac.kr (S.J.); provenance@cau.ac.kr (S.S.); sksdoe@cau.ac.kr (J.H.P.); kenaz93@cau.ac.kr (J.K.); sjss555@cau.ac.kr (S.K.); gkdlsjfl@cau.ac.kr (S.L.); sinkim@cau.ac.kr (S.K.)

[2] Research Center for Safe Nuclear System, Institute for Integrated Radiation and Nuclear Science, Kyoto University, Asashiro-nishi, Kumatori-cho, Sennan-gun 590-0494, Osaka, Japan; pyeon.cheolho.4z@kyoto-u.ac.jp

* Correspondence: bslee@cau.ac.kr

Abstract: Radiation possesses inherent physical characteristics, such as penetrability and radionuclide energy, which enable its widespread applicability in fields such as medicine, industry, environment, security, and research. Advancements in scintillator-based radiation detection technology have led to revolutionary changes by ensuring the safe use and precise measurement of radiation. Nevertheless, certain fields require higher scintillation yields to obtain more refined and detailed results. Therefore, in this study, we explored inorganic scintillators coated with perovskite nanomaterials to detect gamma rays with high light yields. By mixing perovskite with a polymer, we improved the intrinsic characteristics of quantum dots, which otherwise failed to maintain their performance over time. On this basis, we investigated the interactions among inorganic scintillators and a mixed material (CsPbBr3 + PMMA) and confirmed an increase in the scintillation yield and measurement trends. Furthermore, optimized scintillation yield measurement experiments facilitated gamma spectroscopy, demonstrating the validity of our approach through the analysis of the peak channel increases in the energy spectra of various gamma sources in relation to the increased scintillation yield.

Keywords: perovskite; inorganic scintillator; gamma-ray source; photon counting; fluorescence resonance energy transfer

Citation: Jegal, S.; Song, S.; Park, J.H.; Kim, J.; Kim, S.; Lee, S.; Pyeon, C.H.; Kim, S.; Lee, B. Perovskite Nanocrystal-Coated Inorganic Scintillator-Based Fiber-Optic Gamma-ray Sensor with Higher Light Yields. *Photonics* **2024**, *11*, 936. https://doi.org/10.3390/photonics11100936

Received: 16 August 2024
Revised: 28 September 2024
Accepted: 29 September 2024
Published: 4 October 2024

1. Introduction

Radiation possesses inherent physical characteristics, such as the penetrability and energy of radionuclides, which enable its widespread applicability in fields such as medicine, industry, environment, security, and research. Advancements in scintillator-based radiation detection technology have led to revolutionary changes by ensuring the safe use and precise measurement of radiation [1]. However, some fields require higher scintillation yields to obtain more detailed and accurate results using scintillator-based measurement methods.

In medical imaging, gamma rays pass through the body during computed tomography (CT) and positron emission tomography (PET) scans, interact with radiotracers, and transfer the emitted energy to scintillators to produce digital images. During this process, especially for early-stage cancers and tumors that are extremely small, higher scintillation yields and high-resolution images are required. Similar improvements are required when analyzing the detailed structures of blood vessels, such as those in the brain and heart. Therefore, increasing the scintillation yield of scintillators can enhance the measurement efficiency by improving the signal-to-noise ratio, thereby reducing noise and providing spatial resolution images [2]. This process maintains sufficient image quality while reducing the amount of radiation, which is advantageous for pediatric patients and for those requiring repeated examinations to minimize radiation exposure [3].

In gamma-ray spectroscopy, gamma rays emitted from radionuclides interact with scintillators, and the emitted light is used to construct an energy spectrum. Although the energy spectrum results for radionuclides such as Cs-137 and Co-60 yield distinct peak energies (662, 1173, and 1332 keV), other radionuclides such as Ba-133 have less distinct peak regions [4]. In these cases, increasing the scintillation yield improves the energy resolution, making it possible to analyze previously indistinguishable regions and enhancing the ability to measure low-energy regions that are difficult to detect owing to the noise of the measuring device.

As previously mentioned, increasing the scintillation yield to enhance the scintillator measurement efficiency remains a significant future task for achieving the goals of these applications. In this study, we devised a method to increase the light yield of inorganic scintillators, which are commonly used in radiation detection, by coating them with perovskite materials. The properties of the perovskite nanocrystals were improved by mixing them with a polymer (polymethyl methacrylate [PMMA]). Photon-counting experiments demonstrated that the scintillation yields increased owing to the fluorescence resonance energy transfer (FRET) occurring within the scintillators coated with these materials. Additionally, we conducted gamma-ray spectroscopy using the optimal scintillator combination that exhibited the highest increase in light yield. We evaluated the system by analyzing the change in peak resolution indicated by the shift (increase) in the photopeak in the energy spectrum of the radionuclides.

Recent studies have increasingly focused on fabricating liquid scintillators by mixing perovskite materials to detect gamma and X-rays, with continued performance comparisons to conventional scintillators [5]. However, liquid scintillators typically exhibit relatively low light yields, limiting their effectiveness in dose measurement and radiation imaging. In contrast, our study proposes a system in which the materials are simply coated onto the scintillators, eliminating the need for separate experimental setups required for material mixing.

2. Materials and Methods

Perovskite materials have an ABX3 chemical composition, which allows for different materials with varying emission peaks based on their composition. In this study, CsPbBr3 perovskite (Perovskite ABX3 Quantum Dots 510 nm, Quantum Solutions, Southampton, UK) with an emission peak at 510 nm was used.

The perovskite nanocrystals used in this study were characterized by transmission electron microscopy (TEM), and their uniform size distribution with an average diameter of approximately 10 nm can be observed in Figure 1, based on the characterization provided by the supplier.

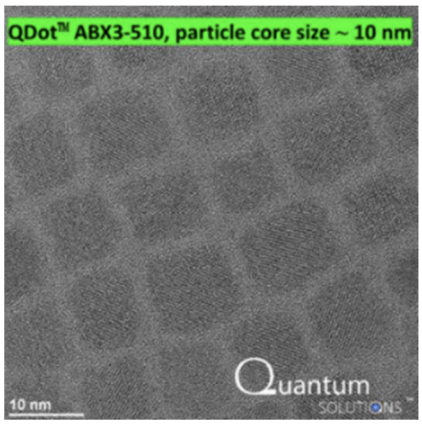

Figure 1. Transmission electron microscopy (TEM) images of perovskite nanocrystals.

Table 1 summarizes the key properties and emission peaks of various compositions of perovskite materials [6].

Table 1. Properties of perovskite quantum dots.

Core Type	Emission Peak	Average Core Size	Photoluminescence Quantum Yield
$CsPb(Cl/Br)_3$	450 ± 5 nm	7 nm	>60%
$CsPb(Cl/Br)_3$	480 ± 5 nm	9 nm	>70%
$CsPbBr_3$	510 ± 5 nm	10 nm	>80%

We experimentally examined perovskite materials with emission peaks at 450 and 510 nm and compared the results. The perovskite material with a 450 nm emission peak showed no difference in photon count before and after coating, even when mixed with a polymer. This lack of improvement is likely because of the decreased performance stability associated with the lower amounts of bromine (Br) in the perovskite composition. Conversely, a significant increase in light emission was observed only for the perovskite material with a 510 nm emission peak.

Quantum dots (QDs) are extremely small semiconductor particles (nanocrystals) with unique electron and hole energy levels that allow them to absorb and emit light at specific wavelengths. These properties vary as a function of the size and structure of the QDs; typically, smaller QDs emit light at shorter wavelengths, while larger QDs emit light at longer wavelengths [7]. QDs are primarily made from semiconductor materials such as CdSe, CdTe, and PbS, which exhibit excellent luminescence properties, making them highly suitable for optical applications [8]. In addition, QDs have high luminous efficiency and outstanding photostability.

However, over time, the photoluminescent properties of QDs can degrade. The degradation process is shown in Figure 2.

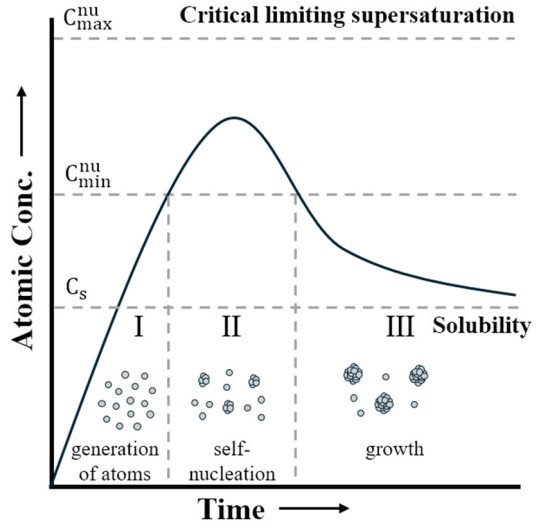

Figure 2. Variation of concentration during nucleation-growth processes.

Figure 2 illustrates the changes in the concentration of quantum dots (QDs) dissolved in the solvent over time [9]. Since this study uses pre-synthesized QDs, we skipped the self-nucleation phase and focused solely on the growth process. As time passes and the concentration drops below Cs, the remaining atoms contribute only to the growth phase, causing further aggregation. This aggregation reduces the overall photoluminescence properties of the nanocrystals. To mitigate this, PMMA is introduced as a polymer matrix, which stabilizes the QDs by preventing them from clumping together. The polymer's chain structure helps ensure that the QDs remain well dispersed, preserving their optical properties [10,11].

As shown in Figure 3, by mixing QDs with polymers, individual nanoparticles can bind to the polymer chains, preventing agglomeration [12,13]. This approach can improve

emission properties. Owing to the characteristics of QDs, the aggregation of the nanoparticles was mitigated by mixing them with a polymer (PMMA, Sigma-Aldrich, St. Louis, MO, USA). The fabrication process of the coating material is illustrated in Figure 4.

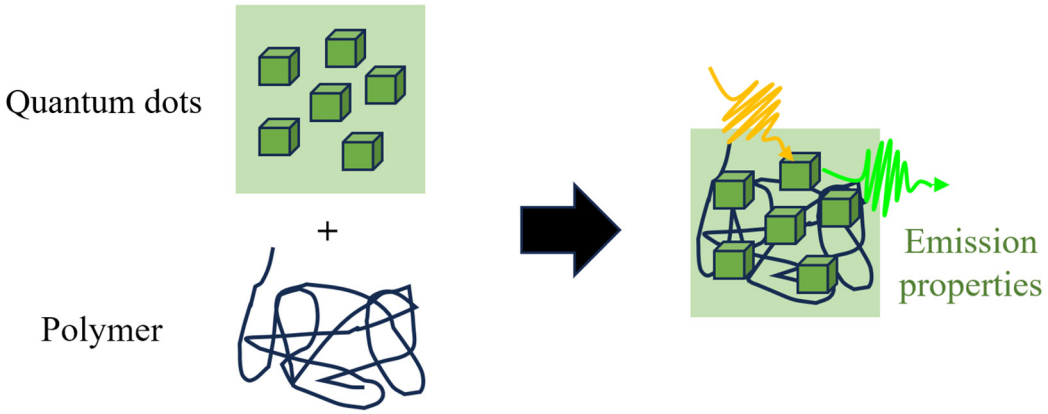

Figure 3. Interaction of quantum dots and polymer. (The yellow arrows in the figure represent the absorbed light, while the green arrows indicate the emitted light.)

Figure 4. Fabrication of coating material.

PMMA was dissolved in toluene to prepare the perovskite as the mixture. This process involved the preparation of solutions at three different concentrations: 30, 50, and 70 mg/mL. While PMMA is inherently soluble in toluene, the dissolution process was accelerated and optimized by heating in a 50 °C oven. The mixture was vigorously stirred at 20 min intervals over a period of 2 h to ensure complete dissolution of the particles. The processes before and after the dissolution are shown in Figure 5.

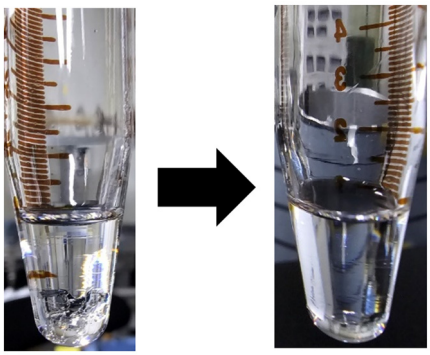

Figure 5. PMMA dissolution process.

The PMMA dissolved in toluene and perovskite was mixed at a 1:1 ratio (0.1 mL each) by stirring for 10 min. The resulting solution (0.2 mL) was spread onto the scintillator, and the solvent was removed by allowing it to dry for 30 min. The coating process and final form are shown in Figure 6 [14].

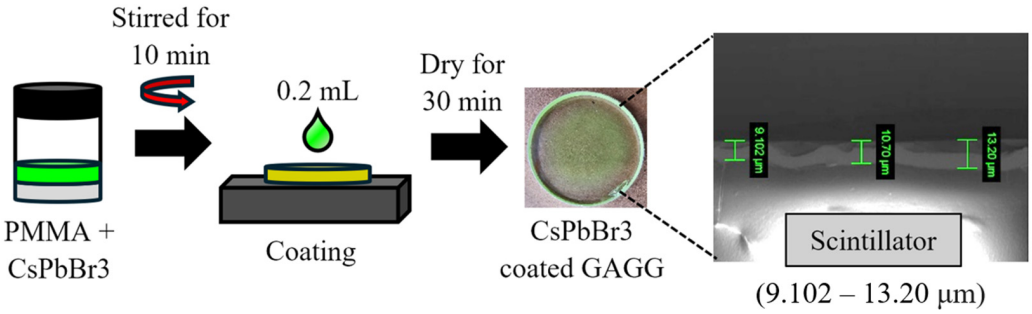

Figure 6. Coating process.

Additionally, scanning electron microscopy (SEM) imaging results confirmed that the coating thickness ranged from 9.102 to 13.2 µm, and the surface morphology of the coating was found to be relatively uneven. While the photon-counting experiment was configured such that the coated surface did not make contact, thus having minimal impact, it is believed that the uneven surface significantly affected the results of the subsequent gamma-ray spectroscopy experiments, where the scintillator was in contact with the PMT window.

FRET refers to the process during which energy absorbed by one molecule is transferred to another molecule when they are physically or chemically connected. This process predominantly occurs at the single-molecule level and results in different fluorescence characteristics depending on the distance and interactions between the molecules.

Typically, the donor molecule initially absorbs light, and this energy is subsequently transferred to the acceptor molecule. After receiving energy from the donor, the donor emits high-energy photons, whereas the acceptor emits low-energy photons.

However, FRET occurs under resonance conditions [15] when a spectral overlap exists between the emission spectrum of the donor and the absorption spectrum of the acceptor and when the distance between the donor and the acceptor is in the range of 1–10 nm.

In this scenario, the light emitted by the donor is directly transferred to the emission region of the acceptor, resulting in an emission spectrum with a considerably enhanced intensity compared with the typical case as shown in Figure 7. Key characteristics include the efficiency of FRET that is maximized when there is a large spectral overlap and the donor–acceptor distance is minimal. In this study, the donor corresponded to the inorganic scintillator, whereas the acceptor corresponded to the perovskite QD.

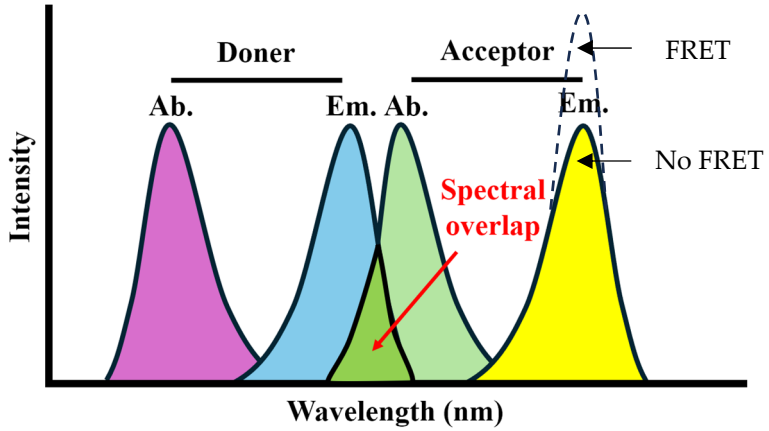

Figure 7. Fluorescence resonance energy transfer (FRET) mechanism.

Inorganic scintillators (GAGG, CdWO4, and LYSO, Epic-Crystal) with a diameter of 25 mm and thicknesses of 1, 3, and 5 mm were utilized. The main characteristics of these scintillators are summarized in Table 2.

Table 2. Properties of inorganic scintillators.

Scintillator	Density (g/cm^3)	Effective Atomic Number	Light Yield (photons/MeV)	Wavelength of Maximum Emission (nm)
GAGG	6.63	54	54,000	530
LYSO	7.25	65	29,000	420
$CdWO_4$	7.90	76	13,000	475

Inorganic scintillators were selected based on the spectral overlap between the donor (scintillator) emission wavelength and the acceptor (perovskite) absorption wavelength, which significantly affects FRET efficiency. To observe clear differences in FRET efficiency, scintillators with peak wavelengths of ~50 nm were selected.

A photon-counting experiment was conducted using the prepared scintillator, as shown in Figure 8. The gamma-ray source was placed inside the connector with the attached coated scintillator, and the emitted photons were transmitted through an optical fiber to the photomultiplier tube (PMT) window of the photon counter (H10682-110, Hamamatsu Photonics, Shizuoka, Japan). The resulting current signal data were used to obtain the photon measurement results.

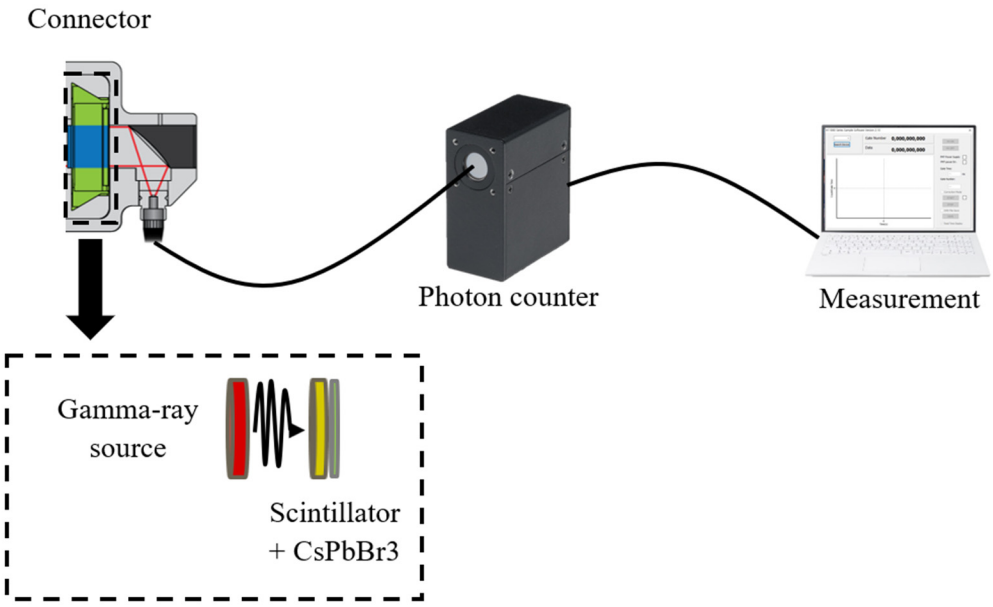

Figure 8. Configuration of photon counting. (The internal structure of the connector is explained in the below.)

Additionally, to evaluate the scintillation increase demonstrated in the photon-counting experiment, we conducted gamma spectroscopy with the highest increase rate combination of concentration and scintillator for each source (Cs-137 and Co-60). The experimental setup is illustrated in Figure 9.

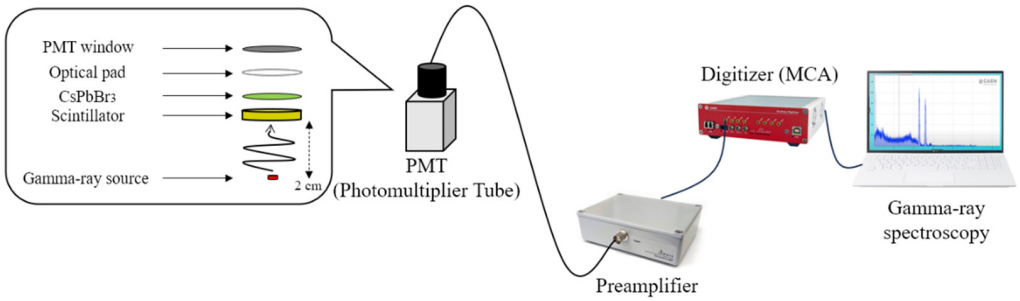

Figure 9. Configuration of the gamma-ray spectroscopy.

In this experiment, the dimensions of each scintillator (which had diameters equal to 25 mm) were maintained consistent with those in the photon-counting experiment. The photometric device used to measure the scintillation signals was a PMT (H10828, Hamamatsu Photonics) with a photocathode area larger than the light-emitting area of the scintillator to ensure complete signal capture [16]. An optical pad (EJ-560, ELJEN Tech., Sweetwater, TX, USA) was used to match the refractive index via direct contact with the PMT window. The current signal generated by the PMT was converted and amplified to a voltage signal using a preamplifier (CR-110, Cremat, Inc., Newton, MA, USA). The amplified signal was analyzed using a digitizer (DT5725, Caen, Viareggio, Italy) that processed the signal peaks to compare the calculated and measured values.

3. Results

3.1. FRET Efficiency

The calculated FRET efficiencies for each scintillator are shown in Figure 10.

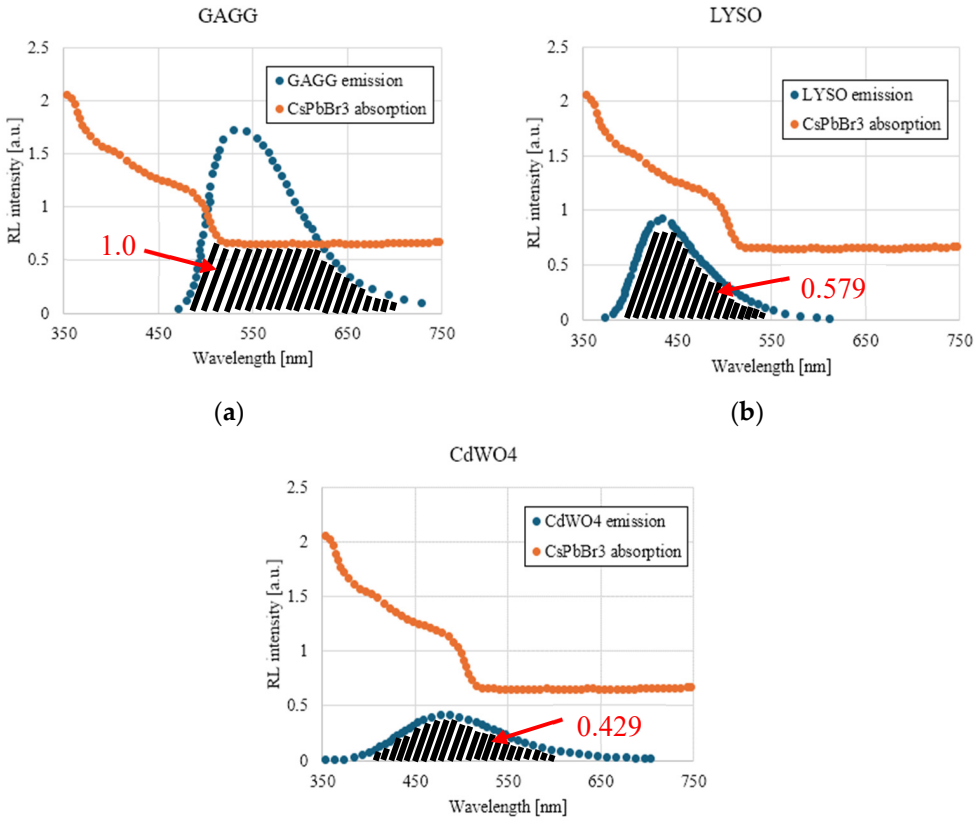

Figure 10. Calculated efficiency of FRET for (**a**) GAGG, (**b**) LYSO, and (**c**) $CdWO_4$.

The spectral overlap areas between the emission wavelengths of each scintillator and the absorption wavelengths of the perovskite were normalized based on the GAGG values. The calculated values for GAGG, LYSO, and CdWO4 were 1.0, 0.579, and 0.429, respectively. It was predicted that the photon-counting values for the coated scintillators would follow the trend in these calculated values, showing an increase in the photon count compared with the uncoated scintillators.

3.2. Photon Counting

The collected optical measurement data were compared based on photon counting and analyzed based on the presence or absence of the coating. One dataset (which spanned 25 min) represents the values measured at 1 s intervals. Measurements were conducted for each source (Co-60 40 µCi, Cs-137 40 µCi); each scintillator (GAGG, CdWO4, LYSO); each thickness (1, 3, 5 mm); and each PMMA concentration examined in this study.

Figures 11 and 12 present the photon-counting data. Overall, it was determined that a concentration of 50 mg/mL resulted in the greatest increase in the photon count. The reason for the distinct differences in the rate of increase with varying concentrations is the varying levels of transmittance and absorbance, which are dependent on the concentration ratio of the CsPbBr3 and PMMA mixture. Consequently, the optimal transmittance was observed when the CsPbBr3 to PMMA ratio was 1:5.

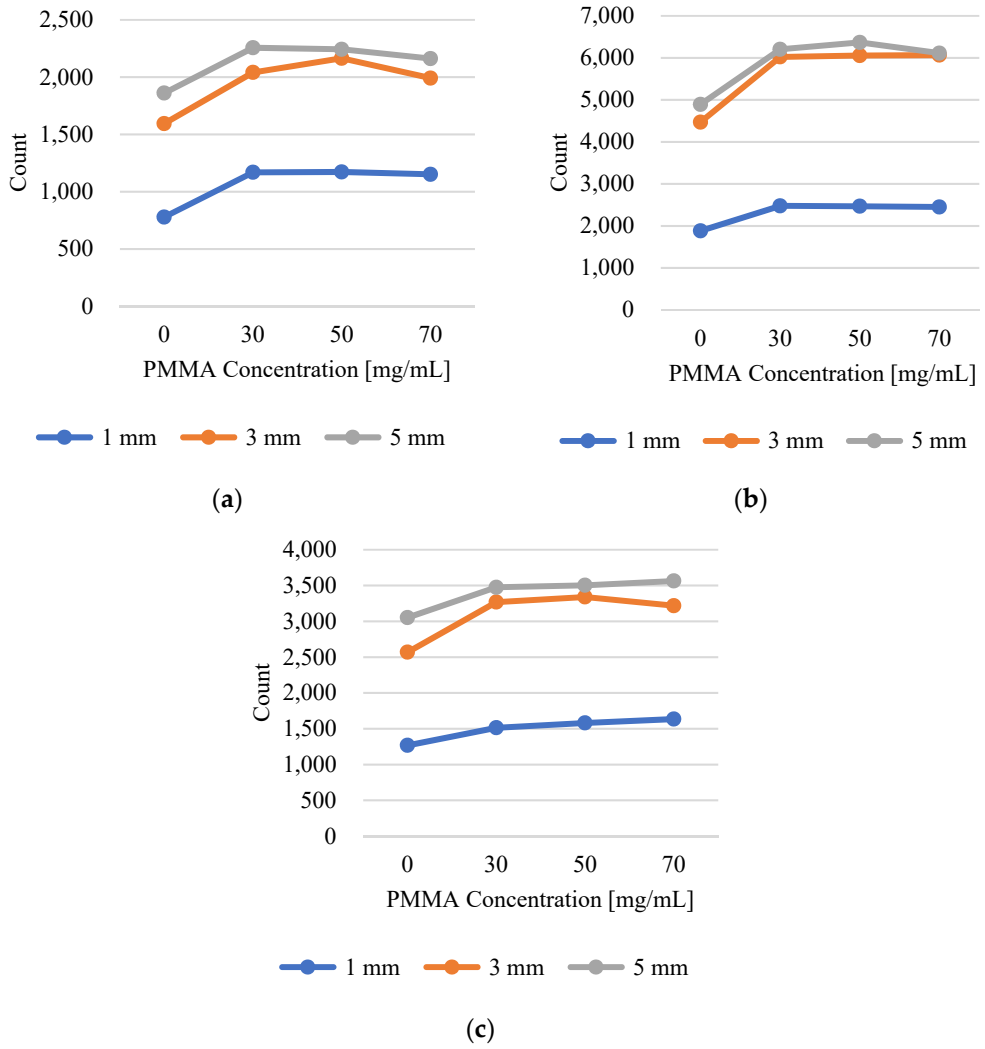

Figure 11. Photon-counting results of Cs-137 40 µCi for (**a**) GAGG, (**b**) LYSO, and (**c**) CdWO4.

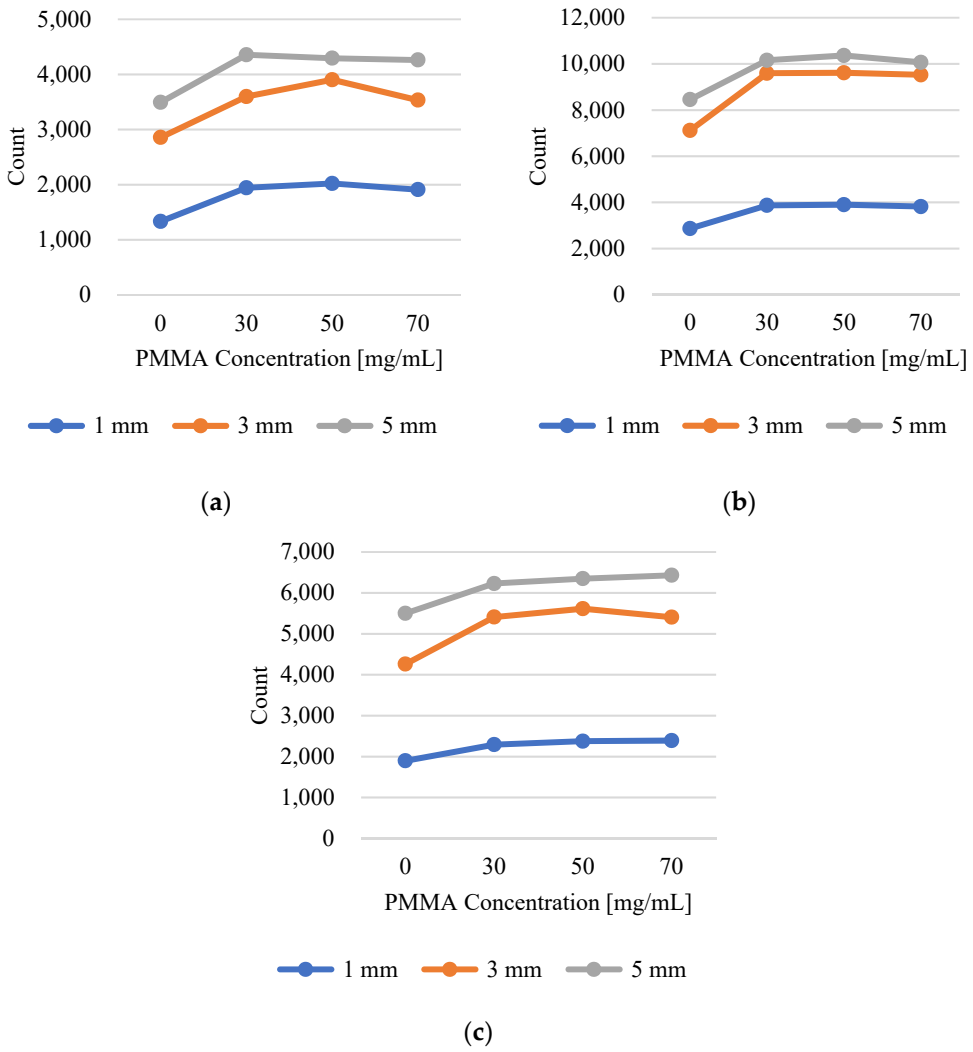

Figure 12. Photon-counting results of Co-60 40 μCi for (**a**) GAGG, (**b**) LYSO, and (**c**) $CdWO_4$.

Table 3 lists the maximum increases for each tested condition.

Table 3. Maximum increase rate.

Scintillator	Gamma-ray Source	Increase Rate (%)	FRET Efficiency
GAGG	Cs-137 Co-60	50.4 51.6	1.0
LYSO	Cs-137 Co-60	35.7 36.9	0.579
$CdWO_4$	Cs-137 Co-60	30.0 32.7	0.429

This trend aligns with the FRET efficiency values calculated based on the emission wavelength and light yield of the inorganic scintillators. The trend of increasing rates of the gamma-ray source and scintillator can also be explained by the mobility of photons and electrons owing to Compton scattering. The maximum range of beta particles is defined by the following equation [17].

$$\begin{aligned} R &= 0.407 \times E_\beta{}^{1.38} \left(0.15 < E_\beta < 0.8\ MeV\right) \\ R &= 0.542 \times E_\beta - 0.133 \quad \left(0.8 < E_\beta\ MeV\right) \\ Maximum\ range &= \frac{R}{Scintillator\ density} \end{aligned} \tag{1}$$

where E_β is the maximum energy of Compton electrons.

Accordingly, the maximum range of beta particles for each source is based on the density of the scintillator.

As evident from the data in Table 3, while the rates of increase for Cs-137 and Co-60 are nearly identical within the same scintillator, a more detailed analysis reveals that Co-60, which has a relatively longer maximum range of beta particles, exhibits a greater increase in the light yield. This discrepancy becomes more pronounced as the scintillator material density increases. When we compared the values calculated for the Cs-137 gamma source using Equation (1), we found maximum ranges of 0.22395 mm, 0.20388 mm, and 0.18710 mm for GAGG, LYSO, and CdWO4, respectively. The uncertainty in determining the maximum range of beta particles was estimated using error propagation techniques. For the Cs-137 source, with a maximum Compton electron energy of 0.477 MeV, the calculated range was 0.1465 cm. The primary sources of uncertainty arose from the beta particle energy ($E\beta$) and the scintillator density, with both assumed to have a ±1% uncertainty. The recalculated uncertainties in the maximum range for GAGG, LYSO, and CdWO4 were ±0.0038 mm, ±0.0034 mm, and ±0.0032 mm, respectively. These uncertainties reflect a 1–2% variation, which aligns with the assumed uncertainties in $E\beta$ and the scintillator densities. As the maximum range of beta particles decreased, the increase in light yield also diminished, indicating a strong correlation between particle range and scintillation efficiency.

This phenomenon can be explained by the fact that with a shorter maximum range, most Compton scattering events occur farther from the coating surface [18] (Figure 13). Consequently, the photons generated from these events must travel a longer distance to reach the coating surface compared with other scintillators. This results in a reduction in the amount of light reaching the coating surface. Therefore, the longer the distance the photons must travel, the lower the light yield observed.

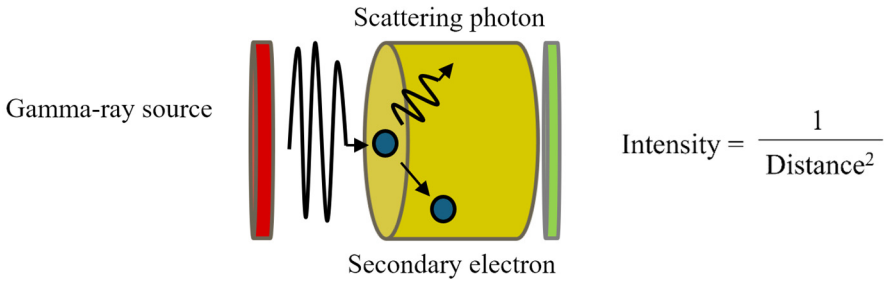

Figure 13. Process of Compton scattering.

3.3. Gamma-ray Spectroscopy

The energy spectrum of the Cs-137 40 μCi source, measured by a GAGG scintillator over 600 s, is shown in Figure 14.

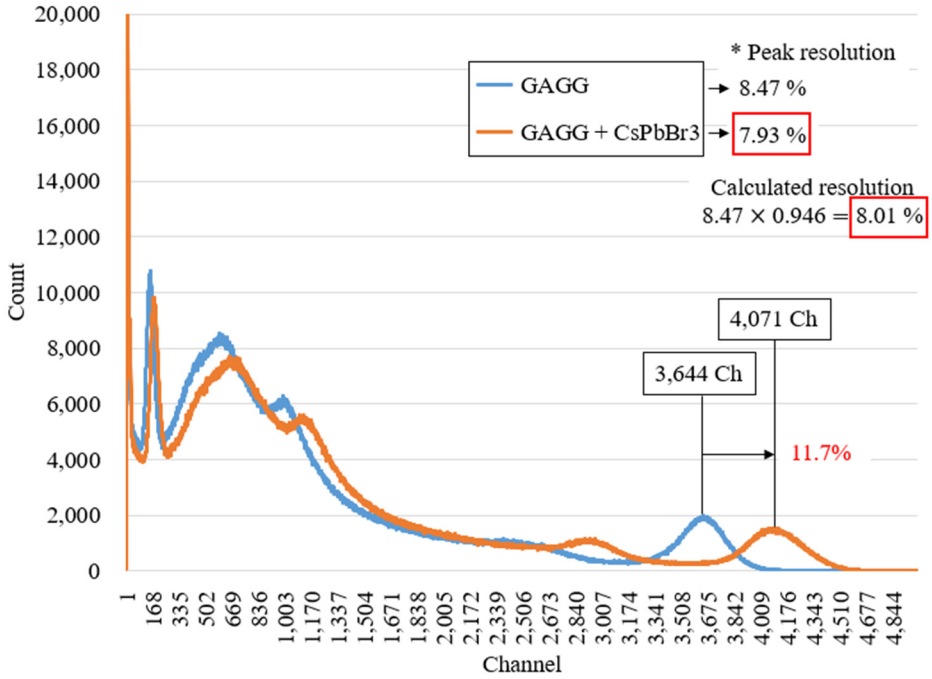

Figure 14. Energy spectrum of Cs-137 measured by GAGG.

The increase in scintillation light owing to the coating of the perovskite material on the scintillator is reflected in the gamma-ray energy spectrum, with an enhancement in the channel position of the peak energy region (e.g., Cs-137 at 662 keV). This shift can be expressed using the following equation [19]:

$$\overline{Q}_0 = \overline{N}\overline{p}\overline{M} \tag{2}$$

where $\overline{Q}_0$ is the amplitude of the PMT output pulse, $\overline{N}$ is the mean number of photons generated by the gamma-ray's interaction with the scintillator, and $\overline{P}$ is the average transfer efficiency, which represents the probability of an electron produced at the first dynode of the PMT by a scintillating photon [20] $\overline{N}\overline{p}$ eventually means the number of photoelectrons produced in the PMT [21,22], and $\overline{M}$ is the multiplication factor [23,24].

In Equation (2), the output pulse refers to the channel value of the energy spectrum. Under ideal conditions, the experimental results indicate that the number of photoelectrons generated by the PMT increases by 11.7%. Consequently, the energy resolution of the peaks improved from 8.47% to 7.93%. Energy resolution is influenced by various factors, including the number of photons measured by the detector and the scintillator characteristics. These variables are typically configured under ideal conditions and the energy resolution is generally expressed as follows:

$$R = 2.35\sqrt{\frac{1 + v(M)}{\overline{N}\overline{p}}} \tag{3}$$

where R is the energy resolution of the scintillation detector, $\overline{N}\overline{p}$ is the number of photoelectrons produced in the PMT, and $v(M)$ is the PMT gain, which is a fixed value determined by the specific PMT used. Therefore, the energy resolution was primarily influenced by the number of photoelectrons generated by the PMT. Upon substituting the derived value of 11.7% from Figure 14 into Equation (3), it was revealed that coating the scintillator with the perovskite material improved the resolution by a factor of 0.946 compared with the original resolution. This resulted in an estimated value of 8.01%, which closely matched the measured value of 7.93% as shown in Figure 14.

Similarly, using the same mechanism, the gamma source Co-60 was evaluated in Figure 15.

Owing to the increased light yield, the number of channels for Cs-137 and Co-60 increased by 11.7% and 16.4%, respectively. Although these values were lower than those observed in the photon-counting experiments, they exhibited a consistent trend. The comparatively lower increase in the channel counts can be attributed to the uneven coating surface, as observed in the SEM images, which likely caused the formation of air gaps during contact with the optical pad, thereby hindering complete light transmission. Additionally, despite the enhanced durability achieved by combining the polymer with perovskite, the coating surface remained prone to damage during contact, which likely affected the results.

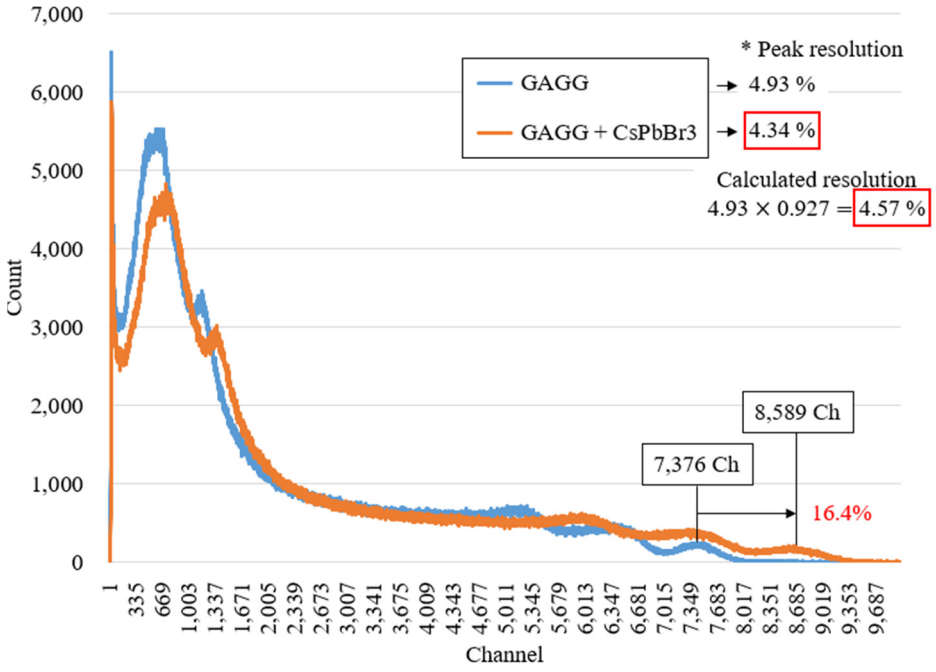

Figure 15. Energy spectrum of Co-60 measured by GAGG.

When the coating was composed solely of the perovskite material without improving the properties of the QDs, the performance stability was too short to obtain results from the photon-counting experiments. Consequently, we evaluated the sustainability of the performance of the coating surface composed of the mixed material by measuring the peak shift in the Cs-137 spectrum using gamma spectroscopy. The details of this evaluation are depicted in Figure 16. The peak channel values for Cs-137, corresponding to 662 keV, were assessed over time, with the differences from the 0 h calculated as a percentage for each time point.

As a result, as shown in Figure 16b, the channel of the peak fluctuated within approximately 1% over a 48-hour period.

In conclusion, this study demonstrated the feasibility of applying gamma spectroscopy to perovskite nanocrystal-coated scintillators.

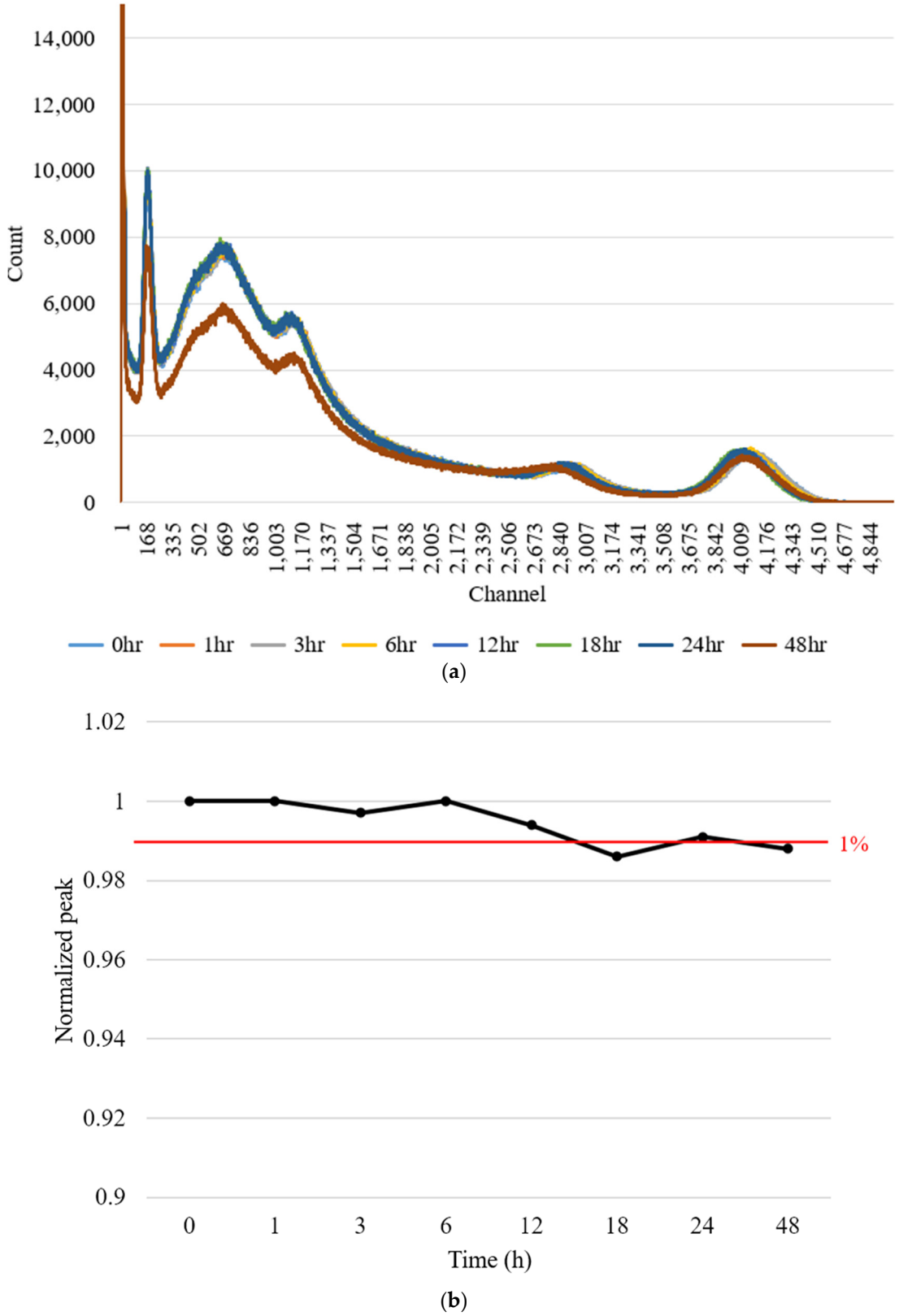

Figure 16. Performance sustainability achieved by shifting the peak of the Cs-137 source. (**a**) shows the energy spectrum results, and (**b**) presents the channel values of the peaks at each time point, normalized to the values at time 0 h.

4. Discussion

Advancements in scintillator-based radiation detection technology have led to revolutionary changes by ensuring the safe use and precise measurement of radiation. Nevertheless, certain fields require higher scintillation yields to obtain more refined and detailed results. In this study, we explored inorganic scintillators coated with perovskite nanomaterials to detect gamma rays with high light yields. By mixing perovskite with a polymer, we improved the intrinsic characteristics of QDs, which otherwise failed to maintain their performance over time. Based on these improvements, we conducted photon-counting experiments and found that the rates of increase were consistent with the FRET efficiency calculations for different scintillators. Consequently, the highest rates of increase were observed with GAGG at 50.4% and 51.6% for Cs-137 and Co-60, respectively. These differences are attributed to the maximum energy of the Compton electrons for each source and the maximum range of beta particles determined by the density of the scintillators.

Based on the results of photon-counting experiments, we optimized the combinations for gamma-ray spectroscopy. The increase in the scintillation yield was reflected in the increased peak channels of the energy spectrum for each source, along with an improvement in the energy resolution. We compared the calculated and measured energy resolutions with and without the coating and found that the values matched closely. Additionally, we assessed the performance stability by analyzing the peak shift in the Cs-137 energy spectrum over 48 h and confirmed that the performance remained stable within approximately 1%. However, the increase in the scintillation yield observed in gamma-ray spectroscopy was lower than that in the photon-counting results. Nevertheless, this experiment demonstrated the feasibility of using perovskite nanocrystal-coated scintillators for gamma spectroscopy. Evidently, the rate of the channel increase varied for each source. This variation could be particularly beneficial in scenarios where multiple sources are measured in contaminated areas and a relatively low resolution may make it challenging to distinguish the peak energies. The ability to differentiate between these increases facilitates accurate identification and measurements in these environments.

5. Conclusions

In this study, we developed a sensor system using scintillators coated with perovskite nanocrystals to verify the increase in light yield through photon counting and gamma spectroscopy. By combining perovskite nanocrystals with PMMA, we improved the intrinsic characteristics of the QDs. Based on these results, we calculated the FRET efficiency based on the spectral overlap of the perovskite nanocrystals and inorganic scintillators. The photon-counting experiments showed that the rate of increase was consistent with the FRET efficiency calculations across different scintillators. In gamma-ray spectroscopy, the increase in the scintillation yield is reflected in the peak channel increase in the spectrum, leading to an improvement in the energy resolution. However, these values were lower than those observed in the photon-counting experiment. This discrepancy is likely due to the uneven surface of the coating, as observed in the SEM images, which causes air gaps during contact with the optical pad, thereby impeding the full transmission of light.

In future work, we will focus on the optimization of the coating method to achieve a more uniform surface, preventing the formation of air gaps during contact with the optical pad in gamma-ray spectroscopy, and ensuring complete light transmission. Further studies will be conducted to identify the increase in scintillation yield for each combination based on photon-counting experiments.

Author Contributions: Conceptualization, S.J. and B.L.; methodology, S.J.; software, S.J.; validation, S.S., J.H.P., J.K., C.H.P., S.K. (Sin Kim) and B.L.; investigation, S.S., J.H.P. and S.L.; resources, S.S., J.H.P. and S.K. (Seunghyeon Kim); writing—original draft preparation, S.J.; writing—review and editing, S.J. and B.L.; visualization, S.K. (Seunghyeon Kim) and S.L.; supervision, B.L.; project administration, S.J.; funding acquisition, B.L. All authors have read and agreed to the published version of the manuscript.

Funding: This research was supported by National Research Foundation of Korea (NRF) grants funded by the Korean government (MSIT), grant numbers 2020M2D2A2062457 and 2022M2D4A1084440.

Institutional Review Board Statement: Not applicable.

Informed Consent Statement: Not applicable.

Data Availability Statement: No new data were created or analyzed in this study. Data sharing does not apply to this study.

Conflicts of Interest: The authors declare no conflicts of interest.

Abbreviations

Abbreviation	Meaning
FRET	Fluorescence resonance energy transfer.
PMMA	Polymethyl methacrylate.
QDs	Quantum dots.
PMT	Photomultiplier tube.
SEM	Scanning electron microscopy.
PET	Positron emission tomography.
CT	Computed tomography.
TEM	Transmission electron microscopy.

References

1. Wang, Z.; Dujardin, C.; Freeman, M.S.; Gehring, A.E.; Hunter, J.F.; Lecoq, P.; Liu, W.; Melcher, C.L.; Morris, C.L.; Nikl, M.; et al. Needs, Trends, and Advances in Scintillators for Radiographic Imaging and Tomography. *IEEE Trans. Nucl. Sci.* **2023**, *70*, 1244–1280. [CrossRef]
2. Enlow, E.; Abbaszadeh, S. State-of-the-art challenges and emerging technologies in radiation detection for nuclear medicine imaging: A review. *Front. Phys.* **2023**, *11*, 6546. [CrossRef]
3. International Atomic Energy Agency (IAEA). Radiation Protection of Children in Radiology. Available online: https://www.iaea.org/resources/rpop/health-professionals/radiology/children (accessed on 25 June 2024).
4. Zhang, D.; Li, X.; Xiong, S.; Li, Y.; Sun, X.; An, Z.; Xu, Y.; Zhu, Y.; Peng, W.; Wang, H.; et al. Energy response of GECAM X and gamma-ray detector prototype. *Nucl. Instrum. Methods Phys. Res. Sect. A* **2018**, *921*, 8–13. [CrossRef]
5. Cho, S.; Kim, S.; Kim, J.; Jo, Y.; Ryu, I.; Hong, S.; Lee, J.-J.; Cha, S.; Nam, E.B.; Lee, S.U.; et al. Hybridisation of perovskite nanocrystals with organic molecules for highly efficient liquid scintillators. *Light Sci. Appl.* **2020**, *9*, 156. [CrossRef] [PubMed]
6. Qunatum Solutions. *Qdot Perovskite ABX3 Quantum Dots: Technical Data Sheet*; Quantum Solutions: Southampton, UK, 2022.
7. Mohamed, W.A.A.; El-Gawad, H.A.; Mekkey, S.; Galal, H.; Handal, H.; Mousa, H.; Labib, A. Quantum dots synthetization and future prospect applications. *Nanotechnol. Rev.* **2021**, *10*, 1926–1940. [CrossRef]
8. Gidwani, B.; Sahu, V.; Shukla, S.S.; Pandey, R.; Joshi, V.; Jain, V.K.; Vyas, A. Quantum dots: Prospectives toxicity, advances and applications. *Deliv. Sci. Technol.* **2021**, *61*, 102308. [CrossRef]
9. Cotin, G.; Heinrich, B.; Perton, F.; Kiefer, C.; Francius, G.; Mertz, D.; Freis, B.; Pichon, B.; Strub, J.; Cianférani, S.; et al. A Confinement-Driven Nucleation Mechanism of Metal Oxide Nanoparticles Obtained via Thermal Decomposition in Organic Media. *Small* **2022**, *18*, e2200414. [CrossRef] [PubMed]
10. Yang, X.; Xu, T.; Zhu, Y.; Cai, J.; Gu, K.; Zhu, J.; Wang, Y.; Shen, J.; Li, C. Preparation of $CsPbBr_3$@PS composite microspheres with high stability by electrospraying. *J. Mater. Chem. C* **2018**, *6*, 7971–7975. [CrossRef]
11. Song, L.; Guo, X.; Hu, Y.; Lv, Y.; Lin, J.; Liu, Z.; Fan, Y.; Liu, X. Efficient Inorganic Perovskite Light-Emitting Diodes with Polyethylene Glycol Passivated Ultrathin $CsPbBr_3$ Films. *J. Phys. Chem. Lett.* **2017**, *8*, 4148–4154. [CrossRef] [PubMed]
12. Fanizza, E.; Schingo, R.; Panniello, A.; Lanza, A.M.; Depalo, N.; Agostiano, A.; Curri, M.L.; Striccoli, M. $CsPbBr_3$ Nanocrystals-Based Polymer Nanocomposite Films: Effect of Polymer on Spectroscopic Properties and Moisture Tolerance. *Energies* **2020**, *13*, 6730. [CrossRef]
13. Chen, L.-C.; Tien, C.-H.; Tseng, Z.-L.; Dong, Y.-S.; Yang, S. Influence of PMMA on All-Inorganic Halide Perovskite $CsPbBr_3$ Quantum Dots Combined with Polymer Matrix. *Materials* **2019**, *12*, 985. [CrossRef] [PubMed]
14. Děcká, K.; Král, J.; Hájek, F.; Průša, P.; Babin, V.; Mihóková, E.; Čuba, V. Scintillation Response Enhancement in Nanocrystalline Lead Halide Perovskite Thin Films on Scintillating Wafers. *Nanomaterials* **2021**, *12*, 14. [CrossRef] [PubMed]
15. Broussard, J.A.; Green, K.J. Research Techniques Made Simple: Methodology and Applications of Förster Resonance Energy Transfer (FRET) Microscopy. *J. Investig. Dermatol.* **2017**, *137*, e185–e191. [CrossRef] [PubMed]
16. Hamamatsu Photonics K.K. *Photomultipier Tubes: Basic and Applications*; Hamamatsu Photonics K.K.: Shizuoka, Japan, 2017.
17. Segre, E. The passage of radiations through matter, Energy Loss of Electrons. In *Nuclei and Particles*, 2nd ed.; W.A. Benjamin, Inc.: New York, NY, USA, 1964; p. 26.

18. Knoll, G.F. Interaction of Gamma Rays, Compton Scattering. In *Radiation Detection and Measurement*, 4th ed.; John Wiley & Sons, Inc.: Hoboken, NJ, USA, 2010; p. 49.
19. Samedov, V.V. Why Do We Need a Standard Theory of Scintillation Spectrometers with Several Photodetectors? *Phys. At. Nucl.* **2021**, *84*, 1713–1728. [CrossRef]
20. Dorenbos, P.; de Haas, J.T.M.; van Eijk, C.W.E. Non-proportionality in the scintillation response and the energy resolution obtainable with scintillation crystals. *IEEE Trans. Nucl. Sci.* **1995**, *42*, 2190–2202. [CrossRef]
21. Dorenbos, P. Light output and energy resolution of Ce3+-doped scintillators. *Nucl. Instrum. Methods Phys. Res.* **2002**, *486*, 208–213. [CrossRef]
22. Khodyuk, I.V.; Dorenbos, P. Nonproportional response of LaBr3:Ce and LaCl3:Ce scintillators to synchrotron x-ray irradiation. *J. Phys. Condens. Matter.* **2010**, *22*, 485402–485408. [CrossRef] [PubMed]
23. Kuntner, C.; Auffray, E.; Lecoq, P.; Pizzolotto, C.; Schneegans, M. Crystal Clear Collaboration, Intrinsic energy resolution and light output of the Lu0.7Y0.3AP:Ce scintillator. *Nucl. Instrum. Methods Phys. Res.* **2002**, *493*, 131–136. [CrossRef]
24. Birks, J.B. *The Theory and Practice of Scintillation Counting*, 1st ed.; Pergamon: New York, NY, USA, 1967.